Potential of Thermochemical Energy Storage for Industrial Heat Demand in Europe Based on a Modular Reactor of Calcium Looping

A. Marques-Valderrama[a], J.M. Guisado[a], I. Marques-Valderrama[a], C. Ortiz[b], J.A. Becerra[a,c] and R. Chacartegui[a,c]

[a] *University of Seville, Seville, Spain*
[b] *Universidad Loyola Andalucía, Seville, Spain*
**Corresponding author: amarques@us.es*

Abstract:

Industrial heat accounts for nearly two-thirds of total industrial energy demand, with a significant share required at high temperatures. Decarbonizing these hard-to-abate processes requires flexible energy storage solutions capable of integrating intermittent renewable sources. This work presents a techno-economic assessment of Calcium Looping (CaL) thermochemical energy storage (TCES) systems deployed across six representative climatic zones in Europe. The analysis is supported by a specific cost-decomposition model for the CaL reactor, rather than relying on conventional volumetric or power scaling laws. Through hourly modeling of mass and energy balances over a full year, the system's capacity to buffer fluctuations in photovoltaic and wind power is evaluated to meet steady industrial thermal loads. Results show that the system can cover more than 80% of the annual industrial heat demand in the majority of the scenarios, achieving near 100% supply through optimized operational strategies. Concurrently, the Levelised Cost of Heat (LCOH) fluctuates dynamically as a function of the local renewable energy scenario, yielding a viable range of 150–175 €/MWh across most analyzed regions, which is highly driven by regional electricity pricing and local solar-wind resource synergy. The study provides a scalable framework for the optimal deployment of TCES, demonstrating the potential of this technology to bridge the gap between variable renewable supply and the rigid operational requirements of high-temperature industrial sectors in Europe.

Keywords:

Thermochemical Energy Storage; Industrial Heat Demand; Calcium Looping

1. Introduction

The decarbonisation of the industrial sector represents one of the most critical challenges in achieving climate neutrality at both European and global scales. Industry is responsible for approximately 25% of the total final energy consumption in the European Union, with thermal processes dominating this demand profile. Heat accounts for nearly half of global final energy consumption and approximately 38% of energy-related CO_2 emissions [1]. Within industry, thermal energy represents close to two-thirds of total energy use, corresponding to more than 1300 TWh of annual industrial heat demand in Europe alone, with a significant fraction required at medium and high temperatures above 400 °C [2].

Despite the rapid expansion of renewable electricity generation, the decarbonisation of industrial heat remains limited, particularly in hard-to-abate sectors such as steel, cement, chemicals, and pulp and paper. These industries require continuous, high-grade thermal energy streams that are difficult to electrify directly using current technologies. While electrification solutions such as industrial heat pumps provide a viable pathway for low-temperature applications, their operational range is typically restricted to below 200 °C, leaving a substantial gap for high-temperature processes [3].

Renewable energy sources, particularly photovoltaic (PV) and wind power, are expected to play a central role in the decarbonisation of industrial systems due to their decreasing levelised cost and widespread deployment. However, their inherent variability and intermittency create a fundamental mismatch between energy supply and industrial demand profiles. This temporal misalignment poses a significant challenge for industrial applications, which typically require stable and continuous heat input to ensure process reliability and efficiency. Furthermore, studies have demonstrated that the variability of wind and solar resources can

significantly impact system costs, emissions, and operational stability, particularly under high penetration scenarios [4].

Thermal energy storage (TES) technologies have emerged as a key enabling solution to bridge this gap by decoupling energy generation from consumption and enhancing system flexibility. TES systems allow the storage of excess renewable energy during periods of high generation and its release during demand peaks, thus enabling a higher penetration of variable renewable energy sources in industrial processes [5]. Among the different TES technologies, sensible and latent heat storage systems are commercially available but are generally limited by low energy density, thermal losses, and temperature constraints. In contrast, thermochemical energy storage (TCES) systems offer higher energy density, negligible thermal losses during storage periods, and the capability to deliver heat at high temperatures, making them particularly suitable for industrial applications [6].

Among TCES technologies, calcium looping (CaL) has emerged as a promising candidate due to its favourable characteristics, including low-cost and abundant raw materials, high operating temperature, and high energy density. The process is based on the reversible reaction between calcium carbonate ($CaCO_3$) and calcium oxide (CaO), enabling the storage of energy through an endothermic calcination reaction and its release via an exothermic carbonation reaction. This system can operate at temperatures exceeding 900 °C and has the potential to deliver high-temperature heat suitable for industrial processes [7]. Additionally, calcium looping can be integrated with carbon capture processes, providing an additional pathway for emissions reduction [8], [9].

Despite its potential, the large-scale deployment of CaL-based thermochemical systems remains limited by several technical and economic challenges. These include material degradation due to sintering over multiple cycles, complex reaction kinetics involving both chemical and diffusion limitations, and significant engineering challenges associated with reactor design and heat transfer [10], [11]. Most existing systems rely on fluidised bed reactor configurations, which introduce additional complexity related to solids handling and scale-up [12]. Furthermore, recent studies emphasise that scaling up CaL systems requires addressing critical issues related to gas–solid interactions, reactor integration, and system-level optimisation [13].

In addition to these technical limitations, most existing studies on thermochemical energy storage focus on reactor-level performance or simplified system configurations, often neglecting the spatial and temporal variability of renewable resources. Few works have simultaneously considered the integration of renewable energy supply, industrial heat demand, and system-level techno-economic performance under realistic, hourly resolved operating conditions across different geographic locations.

No previous study has simultaneously integrated a modular fixed-bed calcium looping configuration with spatially resolved renewable energy variability and hourly industrial heat demand profiles across multiple European regions while performing a detailed techno-economic assessment based on Levelised Cost of Heat.

To address these limitations, this study proposes a comprehensive framework for evaluating the integration of a modular calcium looping-based thermochemical energy storage system with renewable energy sources across Europe. The proposed concept is based on a single-reactor fixed-bed configuration designed to reduce system complexity and improve scalability. Six representative European locations are selected to capture a wide range of renewable resource conditions, enabling a spatially resolved assessment of system performance. The analysis combines hourly thermodynamic modelling with a detailed economic evaluation based on the Levelised Cost of Heat (LCOH), considering different renewable energy mixes and industrial demand profiles. By linking renewable variability, thermochemical storage behaviour, and economic performance within a unified framework, this work provides new insights into the role of thermochemical energy storage in enabling the decarbonisation of high-temperature industrial heat across Europe.

2. Industrial Heat Demand and Renewable Potential in Europe

The defossilisation of the hard-to-abate European industrial sector is one of the most critical challenges in the transition toward a climate-neutral economy, primarily due to the substantial share of energy used for thermal processes. Unlike residential heating, industrial heat demand is highly heterogeneous, spanning a wide spectrum of operating temperatures—from low and medium-temperature utilities to high-grade heat exceeding 500 °C required in heavy industries. While Europe possesses significant and expanding renewable energy potential, primarily driven by wind and solar, successfully integrating these clean sources into manufacturing is not a straightforward substitution. It requires aligning the naturally fluctuating, intermittent, and weather-dependent profile of renewable generation with the strict, often continuous, and high-temperature requirements of industrial production. This section analyses the current architecture of Europe's industrial heat demand across its distinct temperature ranges alongside the regional and temporal availability of renewable resources, highlighting the systemic gaps that must be bridged to achieve effective integration.

2.1 Industrial heat demand

Industrial heat represents one of the dominant energy vectors in the industrial sector, accounting for nearly two-thirds of total industrial energy consumption [1]. This demand spans a wide range of temperature levels, from low-grade heat (<200 °C) to high-temperature processes exceeding 1000 °C, particularly in heavy industries such as steel, cement, and chemicals. Several studies have analysed the distribution of industrial heat demand across sectors and temperature ranges in Europe, highlighting the strong concentration of energy consumption in medium- and high-temperature processes above 400 °C [14]. These temperature levels remain particularly challenging to decarbonise, as direct electrification options are currently limited to low-temperature applications [3].

Industrial heat consumption in Europe is characterised by its massive scale and highly diverse operational requirements, making it one of the most complex sectors to decarbonise. Thermal energy accounts for most of the total industrial energy use across the continent, yet this demand is far from uniform; it is strictly segmented by the specific temperature levels required for different manufacturing processes. European industries are crucial, as the temperature level dictates not only the technological feasibility of replacing fossil fuels but also the types of renewable and storage systems capable of supplying it.

To provide a granular understanding of this landscape, it is essential to quantify thermal energy demand for individual manufacturing sectors and their corresponding temperature thresholds. Table 1 delineates European industrial heat demand, categorised by temperature vectors and industrial sectors, revealing how energy use is distributed among electrification, steam networks, and direct non-electric process heat [14]. These data underscore the profound heterogeneity of the market and highlight where the most critical thermal bottlenecks reside.

Table 1 *Industrial Final and Useful Energy Demand by Temperature Level for EU27 and Member States.*

	Electricity Other	Electricity Thermal	Non-electric process heat (<100 ºC)	(100-400 ºC)	(400-1000 ºC)	(>1000 ºC)	Steam (non-electric boilers)
Primary Steel	25,4	0,1	0,3	0,0	4,3	71,4	5,7
Secondary Steel	14,3	23,1	0,2	0,0	7,6	7,8	2,2
Chemicals	53,3	5,1	11,8	0,0	35,4	0,0	125,3
Cement	9,7	0,2	3,0	0,0	24,4	48,4	0,0
Pulp and Paper	46,6	1,5	79,2	0,0	5,0	0,0	119,2
Food, Beverages and Tobacco	33,1	28,1	21,0	6,1	0,0	0,0	75,9
Transport Equipment	13,3	12,5	5,0	0,0	0,0	5,5	10,5
Machinery and Equipment	32,9	29,1	2,0	0,0	10,8	14,3	22,8
Textiles and Leather	4,6	3,2	3,7	0,0	0,0	0,0	7,8
Wood and Wood Products	12,6	1,6	1,8	0,0	0,0	0,0	31,2
Non-ferrous Metals	10,6	21,3	0,2	3,5	0,9	13,9	3,8
Ceramics and Glass	14,6	15,7	1,5	9,1	1,6	90,6	3,3
TOTAL	271,0	141,5	129,6	18,6	90,2	251,9	407,8

Table 1 reveals a clear concentration of energy demand in high-temperature vectors, highlighting the scale of the industrial decarbonisation challenge. Non-electric process heat operating above 400 °C accounts for a massive share of thermal energy consumption, with the 400–1000 °C range requiring 90.2 TWh and temperatures exceeding 1000 °C dominating with 251.9 TWh. Together, these two high-temperature bands constitute a critical pillar of Europe's industrial energy consumption. At the sector-specific level, this high-grade thermal demand is driven primarily by a few core heavy industries. Within the upper 1000 °C range, the primary steel sector accounts for 71.4 TWh due to furnace operations, while the ceramics and glass sector represent the largest single consumer in this specific bracket at 90.6 TWh. Meanwhile, the chemicals and pulp and paper industries stand out as the primary consumers of steam by non-electric boilers, requiring 125.3 TWh and 119.2 TWh respectively, closely followed by the food, beverages and tobacco sector at 75.9 TWh.

The geographic distribution of these thermal requirements across individual European nations is illustrated in the maps below. Figure 1a presents the total industrial heat demand for each member state, and Figure 1c focuses on the temperature ranges in which the proposed energy storage system is most applicable.

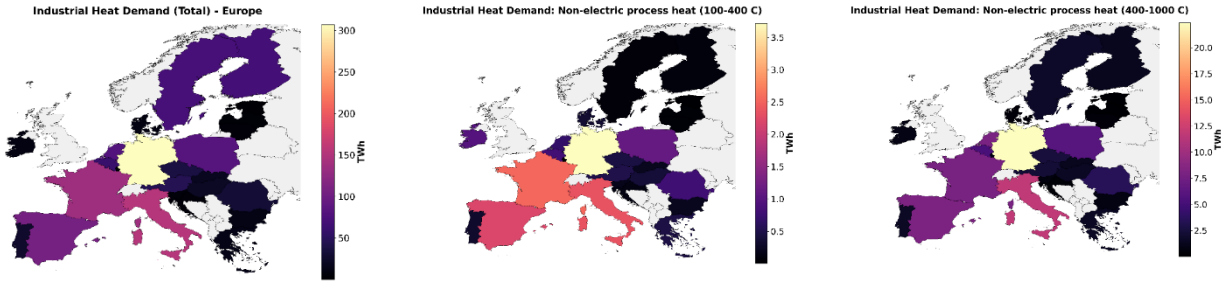

Figure 1 *Industrial Heat Demand in European Union: (a) Total, (b) Non-electric process heat (100-400 ºC) and (c) Non-electric process heat (400-1000 ºC).*

As illustrated in Figure 1a, the total industrial heat demand exhibits a pronounced geographic concentration among a few dominant European economies. Germany stands out as the single largest thermal sink on the continent, with an aggregate demand exceeding 300 TWh. This is followed by a secondary cluster of high-intensity manufacturing nations, primarily France and Italy—ranging from 130 to 170 TWh—and complemented by Spain and Poland in the 80–110 TWh bracket. Conversely, peripheral regions, particularly the Baltic and Scandinavian states, display significantly lower thermal requirements, remaining below 50 TWh. From a strategic perspective, these data indicate that the deployment and commercial viability of large-scale thermochemical energy storage solutions are highly dependent on regional industrial density, with central and southwestern Europe representing the primary target markets.

A comparative assessment of Figures 1b and 1c reveals a significant shift in both the magnitudes of energy and regional distribution as the thermal threshold increases. The non-electric process heat demand in the 400-1000 °C range is nearly six times larger than that in the 100-400 °C bracket, with peak regional consumption rising from under 4 TWh to over 20 TWh. Germany consistently remains the primary thermal sink across both categories, dominating the high-temperature spectrum at over 20 TWh. Notably, a geographical reconfiguration occurs within the secondary manufacturing cluster; while France exhibits a higher demand in the medium-temperature range (100-400 °C), Italy becomes the dominant secondary market in the high-temperature range (400-1000 °C), driven by its intensive non-metallic minerals and metallurgical sectors. This distinct concentration of high-magnitude, high-grade thermal demand underscores the strategic value of high-temperature energy storage systems, as the southwestern and central European corridors present the highest technical potential for such deployments.

The spatial distribution of electrified industrial heat, illustrated in Figure 2a, shows a regional maximum of approximately 30 TWh. Germany exhibits the highest concentration of electro-thermal consumption, exceeding 30 TWh, while the secondary manufacturing tier is led by Italy within the 20-25 TWh bracket, followed by France and Spain. This quantitative baseline indicates that, while electro-thermal technologies have achieved non-negligible deployment in specific regions, their aggregate magnitude remains insufficient to address the core high-temperature thermal blocks identified in Table 1.1. Consequently, these geographical limits underscore the technical constraints of direct industrial electrification, reinforcing the necessity for high-grade thermochemical energy solutions capable of bridging the substantial deficit left by current electrical configurations.

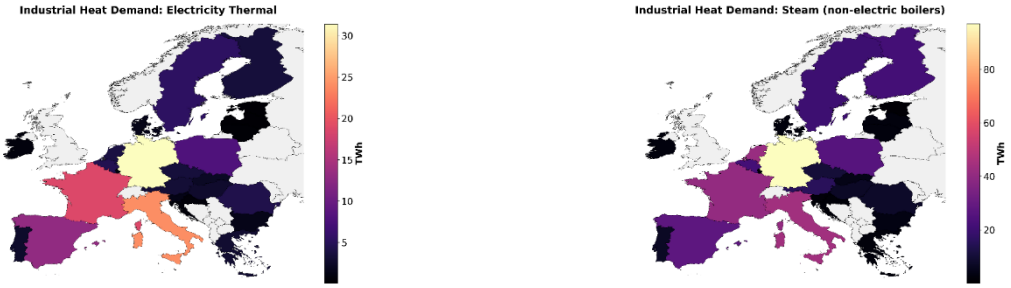

Figure 2 *Industrial Heat Demand: (a) Electricity Thermal and (b) Steam (non-electric boilers)*

The geographic profile of steam demand from non-electric boilers, presented in Figure 2b, provides a critical justification for the strategic deployment of the proposed thermochemical energy storage system. This vector represents a massive share of the European industrial energy fabric, aggregating 407.8 TWh and accounting for over 31% of the total quantified industrial heat demand (1310 TWh). Regionally, Germany represents the most critical thermal sink for this category, with a demand exceeding 90 TWh, followed by a substantial secondary manufacturing cluster led by Italy, France, and Poland. Given that the thermochemical system developed in this study is engineered to deliver steam across both medium and high-temperature ranges, this extensive consumption block represents an optimal market for technology integration. The substantial scale of this utility vector ensures that the deployment of the proposed thermochemical storage architecture directly

addresses the largest consolidated thermal-demand segment in Europe, thereby establishing a technically viable pathway for the deep defossilisation of hard-to-abate industrial processes.

2.2. Matching demand and potential production

To effectively bridge the gap between resource availability and industrial consumption, the operational integration of the proposed thermochemical energy storage system must be evaluated within specific manufacturing contexts. While the macro-scale analysis identifies the aggregate potential across Europe, the technical viability of thermochemical steam generation is ultimately determined by its alignment with the distinct dynamic profiles of high-volume utility consumers. Globally, the chemical, pulp and paper sectors represent the most steam-intensive industrial segments, characterised by continuous, high-grade thermal demands that are traditionally reliant on fossil-fuel boilers. Consequently, this section contextualises the matching framework by analysing two representative benchmarks: styrene production as a proxy for complex chemical synthesis, and large-scale paper manufacturing, establishing a precise techno-economic assessment of how the developed storage architecture can substitute conventional thermal baseloads.

As a representative example within the chemical sector, the catalytic dehydrogenation of ethylbenzene for styrene monomer production [15], [16] illustrates a highly suitable process for integrating the proposed technology, following the technical configuration shown in Figure 3 [17]. In this endothermic process, superheated steam serves as a critical multifunctional utility, supplying the high-temperature sensible heat required to drive the reaction in the catalytic reactor. Simultaneously, the steam acts as a diluent to lower the partial pressures of styrene and hydrogen, shifting the thermodynamic equilibrium toward higher conversion yields, while inhibiting catalyst deactivation by gasifying carbonaceous residues and preventing coke formation. The proposed thermochemical storage system can replace the conventional fossil-fired heaters shown in Figure 3, thereby directly decarbonising this highly energy-intensive utility stream.

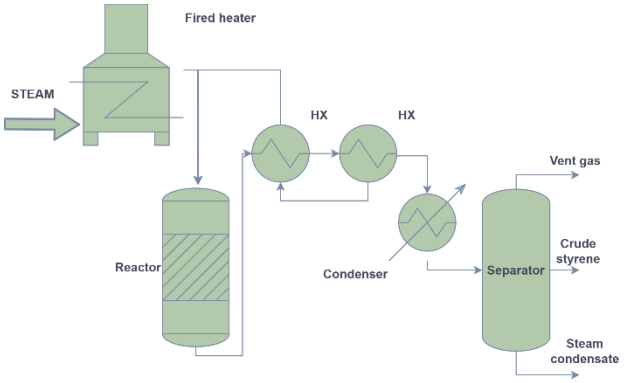

Figure 3 *Catalytic dehydrogenation of ethylbenzene for styrene monomer production*

In the pulp and paper industry[18], [19], steam acts as the primary heat transfer medium[20], serving as an essential utility to maintain the thermal requirements of energy-intensive processes. It is typically supplied at three distinct pressure levels—high, medium and low pressure—to address specific operational needs. Direct steam application is critical in several stages, most notably in pulp bleaching, where it is utilized to reach required process temperatures, and in the concentration of black liquor within multi-effect evaporator systems, which is vital for raising solids concentration prior to recovery boiler combustion. Furthermore, steam is extensively used in heat exchangers to produce hot water for various process streams, facilitating the integrated thermal management necessary for efficient mill operations.

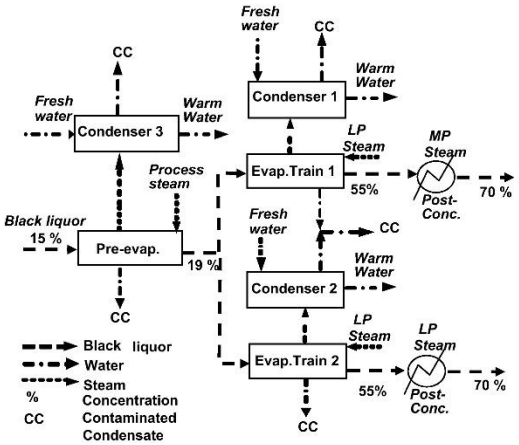

Figure 4 Paper production process. Figure from: *[20]*

3. Thermochemical energy storage

Thermal energy storage (TES) technologies have been widely proposed as a solution to integrate intermittent renewable energy into industrial systems. TES can be classified into sensible, latent, and thermochemical storage systems, each with different technological maturity and performance characteristics [21], [22].

Sensible heat storage is the most mature technology, commonly implemented using molten salts or packed beds. However, its relatively low energy density and thermal losses limit its applicability for long-duration storage. Latent heat storage improves energy density through phase change materials but introduces challenges related to heat transfer and material stability.

Thermochemical energy storage (TCES) offers significantly higher energy density and negligible heat losses, making it particularly attractive for high-temperature industrial applications. However, its deployment remains limited by reactor complexity, material degradation, and integration challenges [23].

Although calcium looping has demonstrated strong potential for high-temperature energy storage, most existing studies are limited to reactor-level analyses or steady-state operating conditions. Furthermore, the majority of CaL systems are based on fluidised bed reactors, which introduce significant complexity in terms of solids handling and scale-up [24]. These limitations highlight the need for alternative configurations that simplify system design while maintaining performance, particularly for industrial-scale deployment.

2.5. Process flow diagram

This section presents the Process Flow Diagram (PFD) of the proposed technology, detailing the novel modular thermochemical energy storage system based on the reversible reaction of Calcium Looping. The concept features a single, highly scalable fixed-bed reactor configuration in which both calcination and carbonation reactions occur. To ensure modularity, transportability, and rapid on-site installation, these fixed-bed reactors are housed inside standard containers, each housing multiple reactors with an internal diameter of 1.3 meters and a height of 2 meters. Renewable power from photovoltaic or wind assets is utilised as the primary energy source to drive the endothermic charging phase, during which the CaCO3 bed undergoes calcination. The released CO2 is extracted, cooled, and routed through a specialised two-stage parallel compressor configuration with intercoolers, then stored in a liquid state at 75 bar and 25 °C. To maximise both chemical conversion and sensible heat storage while preventing solid sintering, the maximum bed temperature is strictly capped at 1100 °C.

During the exothermic discharge phase, the stored CO2 is expanded through a turbine down to 1.2 bar, preheated using the reactor outlet stream, and reinjected into the fixed-bed reactors to react with the accumulated CaO. The system kinetics allow the bed to reach its maximum chemical conversion within 1 hour, generating a high-temperature thermal output suitable for industrial steam production. Any unreacted CO2 leaving the reactor is re-compressed and returned to the high-pressure storage tank. By adopting a modular fixed-bed architecture rather than a fluidised regime, the system eliminates complex solid transport mechanisms and hydrodynamic spatial gradients. This design significantly simplifies factory assembly, standardized testing, and scalable replication, providing a clear pathway to advance the technology readiness level for heavy industrial applications.

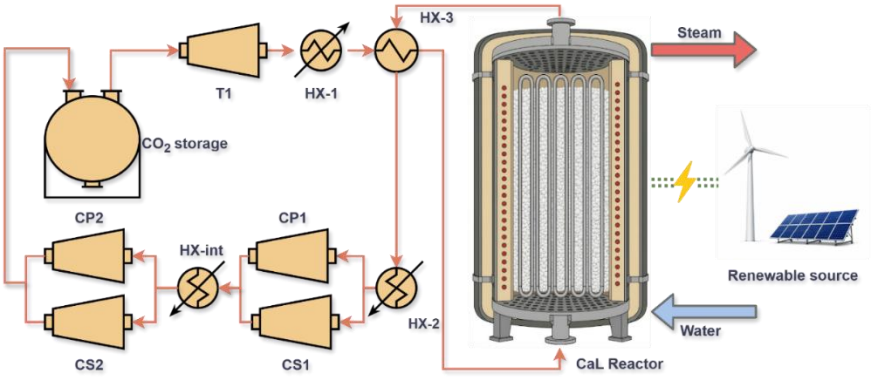

Figure 5 *Process Flow Diagam*

2.5. Reaction and energy balance

The mathematical formulation of the system is detailed in this section. To determine the thermodynamic properties of the process, mass and energy balances were developed in MATLAB, utilising Aspen Properties and CoolProp. The simulation structure is built upon three core pillars: mass balance, energy balance, and techno-economic analysis. All balances are computed sequentially for each hour of the year, using the index i as the hourly counter. The TCES system is based on the reversible calcium looping reaction:

$$CaCO_3 \leftrightarrow CaO + CO_2\ ;\ \Delta H = 178\ \text{kJ/mol} \quad (1)$$

2.5.1. Mass balance

The total solid inventory within the reactor is governed by a combination of physical and structural parameters. Specifically, the total mass of solids is determined as a function of the individual densities of CaCO3 and CaO, the reactor volume, the packing density (PD), and the internal porosity of the CaO matrix.

$$m_{ave}^{reactor} = V^{reactor} \cdot \rho_{ave}^{storage} \quad (2)$$

$$m_{ave}^{total} = n_{containers} \cdot m_{ave}^{reactor} \quad (3)$$

$$m_{0,j} = X_{0,j} \cdot m_{ave}^{total} \quad (4)$$

$$\rho_{ave}^{storage} = \rho_{ave}^{material} \cdot PD \quad (5)$$

$$\rho_{ave}^{material} = \rho^{CaO} \cdot \emptyset^{CaO} \cdot X_{0,CaO} + \rho^{CaCO_3} \cdot X_{0,CaCO_3} \quad (6)$$

Where PD represents the packing density, set to 0.6 for the current model. The porosity of CaO, denoted as ØCaO, is set to 0.5 in accordance with literature data [25]. Furthermore, the volume occupied by the solids is determined by the reactor's internal geometry. The designed reactor features an internal diameter of 1.3 m and a height of 2 m, yielding a total container volume of 2.655 m3. Based on the reaction stoichiometry, the mass in each hourly section will be as follows.

$$m_{reac}^{CaO}(i) = X_{carb}^{conversion}(i) \cdot m^{CaO}(i-1) \quad (7)$$

$$m_{reac}^{CaCO_3}(i) = m_{reac}^{CaO}(i) \cdot \frac{M_m^{CaCO_3}}{M_m^{CaO}} \quad (8)$$

$$m_{reac}^{CO_2}(i) = m_{reac}^{CaO}(i) \cdot \frac{M_m^{CO_2}}{M_m^{CaO}} \quad (9)$$

$$m_j(i) = m_j(i-1) \pm m_{reac}^{j}(i) \quad (10)$$

Where $X_{carb}^{conversion}$ represents the degree of conversion of the carbonation reaction, which, according to the established hypotheses, falls within the range of 0 to 0.15. The term Mm denotes the molar mass of each respective compound, while m_{reac}^{x} represents the reacting mass of each component, where x signifies $CaCO_3$, CaO, or CO2. Consequently, the masses of $CaCO_3$ and CaO within the reactor vary over time as described by Equations 7 and 8.

2.5.1. Energy balance

The thermal behaviour and core thermodynamic interactions of the system are governed by the primary energy exchanges occurring within the reactors. The energy exchanges within the system are modelled using the equations presented below. The process is defined by two thermochemical pathways: the endothermic calcination reaction and the exothermic carbonation reaction (Equation 1). When calcination conditions exist in the reactor—characterized by a temperature above 930 °C and below the maximum reactor temperature, with CaCO3 mass available—the energy required is determined by Equation 11. To track the cyclic evolution of the solid sorbent during this stage, the cumulative conversion state is updated according to Equation 12. Conversely, the energy released in the carbonation process, which occurs at temperatures between 400 and 875 ºC, is defined according to Equation 18.

$$Q_{calc}(i) = \Delta H_r(i) \cdot m_{reac}^{CaCO_3}(i) \quad (11)$$

$$X_{cum}(i) = X_{cum}(i-1) \cdot (1 - X_{calc}(i)) \quad (12)$$

$$Q_{carb}(i) = \Delta H_r(i) \cdot m_{reac}^{CaCO_3}(i) \quad (13)$$

Where ΔH_r is the reaction enthalpy at the reaction temperature, and X_{calc} represents the degree of calcination. If there is sufficient energy to reach the reactor's maximum degree of calcination, X_{cum} will become 0. X_{cum} will increase as the carbonation reaction progresses, reaching its maximum (X_{max}). Regarding the energy terms, Q_{calc} represents the thermal energy required for the calcination reaction, while Q_{carb} is the energy released in the exothermic reaction of carbonation.

The overall energy balance within the reactor is modelled by accounting for the energy input, the industrial heat demand, the sensible heat of the solid inventory, the thermal energy carried by the entering and exiting CO2 streams, and the thermal losses. The net energy balance is governed by Equation 14:

$$Q_{balance}(i) = Q_{PV}(i) - Q_{demand(i)} - Q^{CO_2}(i) - Q^{loss}(i) \quad (14)$$

The sensible heat of the system represents the net thermal energy available to be exchanged or contributed to the chemical transformations. Since the carbonation and calcination reactions never occur simultaneously, the sensible heat is determined through the energy balance and the respective reaction heats, as expressed

in Equation 15. Alternatively, this sensible heat can be quantified based on the temperature variation of the solid phase between consecutive time steps, according to Equation 16:

$$Q_{sensible}(i) = Q_{balance(i)} + Q_{carb}(i) - Q_{calc}(i) \quad (15)$$

$$Q_{sensible}(i) = \sum_{j=Cao,CaCO_3} m_j(j) \cdot cp^j(i) \cdot \left(T^{reactor}(i) - T^{reactor}(i-1)\right) \quad (16)$$

The thermal energy transported by the carbon dioxide streams entering and leaving the reactor is defined by Equation 17:

$$Q^{CO_2}(i) = m_{in}^{CO_2}(i) c_p^{CO_2}(i) \cdot T_{in}^{CO_2}(i) - m_{out}^{CO_2}(i) \cdot c_p^{CO_2}(i) \cdot T_{out}^{CO_2}(i) \quad (17)$$

Thermal losses to the surroundings are assumed to be proportional to the thermal state of the solids, being defined as 0.5% of the sensible heat:

$$Q^{loss}(i) = 0.005 \cdot Q_{sensible}(i) \quad (18)$$

Finally, to evaluate the total energy state of the system, the total stored heat is defined as the sum of a sensible component (Equation 19) and a thermochemical component (Equation 20). The total energy inventory is then compiled in Equation 21:

$$Q_{sen}^{stored}(i) = \sum_{j=CaO,CaCO_3} m^j(i) \cdot c_p^j(i) \cdot (T_{reactor} - T_{release}^{demand}) \quad (19)$$

$$Q_{chem}^{stored}(i) = \Delta H_r(i) \cdot \frac{M_m^{CaO}}{M_m^{CaCO_3}} \cdot m^{CaO}(i) \cdot X_{cum}(i) \quad (20)$$

$$Q^{stored}(i) = Q_{sen}^{stored}(i) + Q_{chem}^{stored}(i) \quad (21)$$

Where $T_{release}^{demand}$ corresponds to the target temperature required by the industrial heat demand.

The theoretical maximum storable heat (Q_{max}) is defined by the compilation of three distinct thermal contributions. First, it includes the sensible heat required to raise the solid inventory from the minimum heat release temperature (220 °C) up to the calcination temperature (exceeding 930 °C). Second, it accounts for the thermochemical enthalpy associated with the calcination reaction. Third, it incorporates the sensible heat of the resulting calcination products as they are heated from the reaction threshold up to the maximum operational temperature of the reactor (1100 °C). Based on these foundational parameters, the state of charge (SOC) of the system is formulated in Equation 27, while the overall volumetric energy density ($E_{density}$) is expressed in Equation 28.

$$SOC(i) = \frac{Q^{stored}(i)}{Q_{max}} \quad (22)$$

$$E_{density} = \frac{Q_{max}}{V^{reactor} \cdot n^{containers} + V_{CO_2}} \quad (23)$$

2.5.1. Auxiliar equipment management

The auxiliary equipment required to regulate the carbon dioxide streams entering and exiting the storage inventory comprises turbines, compressors, and a network of heat exchangers. To maximize the efficiency of the compression process, a two-stage configuration is implemented to elevate the gas pressure up to 75 bar. The specific power consumption of each compressor and the power output of each turbine are determined using Equations 24 and 25, respectively. Regarding the thermal integration, the performance of the gas-to-gas heat exchanger HX-3 is evaluated according to Equation 26, while the remaining heat-exchanging units within the system are modeled using Equation 27.

$$W_{turbine} = m_{CO_2} \cdot (h_{in} - h_{out}) \cdot \eta_{mec} \cdot \eta_{isen} \quad (24)$$

$$W_{comp} = \frac{m_{CO_2} \cdot (h_{out} - h_{in})}{\eta_{mec} \cdot \eta_{isen}} \quad (25)$$

$$Q_{HX-3} = U \cdot A \cdot F \cdot \Delta T \quad (26)$$

$$Q_{HX} = m_{CO_2} \cdot (h_{out} - h_{in}) \quad (27)$$

3. Economic model

This section outlines the comprehensive framework developed to evaluate the techno-economic viability of the proposed modular energy storage system. This model serves as the basis for determining the overall feasibility of the technology and for establishing the multi-variable calculations required to assess its integration into industrial processes. Within this structural framework, a specific cost correlation for the single-reactor

configuration has been formulated, which integrates its physical dimensions, thermal power output, and electrical consumption. While existing literature frequently evaluates thermochemical systems using broader scaling laws based strictly on thermal capacity, the approach presented here attempts to refine these approximations by accounting for the specific operational variables of a modular unit. By linking these technical sizing parameters directly to economic indicators, the model aims to provide a balanced representation of capital expenditures to analyse the system's realistic potential to deliver high temperatures in industrial applications.

3.1. Calcium looping reactor cost

In the literature, most cost-estimation correlations for the calcium looping reactor are based on the system's thermal power. These equations suppose that if the reaction is improved, the cost of the equipment increases. For a better approximation of the cost estimate for the calcium looping reactor, an equation based on a physically grounded decomposition approach, rather than purely energy-based scaling correlations, is used. In this case, it is made for a fixed-bed reactor. This is required due to the weak coupling between thermal power and equipment size in solid-based thermochemical systems, where reactor geometry and material constraints dominate capital expenditure. The calculation is based on [26], [27], [28].

The total reactor cost is expressed as:

$$c_{reactor} = c_{shell} + c_{refractory} + c_{insulation} + c_{internals} + c_{electric} + c_{heat\ exchager} \quad (28)$$

The external shell cost (C_{shell}). The shell cost coefficient was derived from conventional carbon-steel vessel cost correlations [26], [27], reformulated on a surface-area basis, resulting in values in the range of 800–2000 €/m² (year 2022), which reflects variability in vessel thickness, fabrication method, and material requirements) and a base-case of 10 m2 of surface. A reference value of 1200 €/m2 is considered for the reactor designed. The correction factor for pressure (f_p) is 1 if pressure is lower than 4 bars and 1.1 – 1.5 if pressure is between 5 and 20 bars [27]. The reactor designed is supposed to operate at pressures lower than 4 bars. For security reasons and future utilisation, a pressure factor of 1.4 was used.

$$c_{shell} = 12000 \cdot \left(\frac{A}{10}\right)^{0.6} \cdot f_p \quad (29)$$

The refractory need for the reactor is a mix of silica (SiO_2) and alumina (Al_2O_3) because the maximum temperature will be around 1200 ºC. For this purpose, a quantity of 85% alumina is recommended. Material costs for high-alumina refractories (500 – 800 €/ton) is derived from industrial market data for alumina contents around 85 wt%. For the refractory thickness handbooks [29], [30] recommend 0.2 – 0.3 m. For the calculation, a thickness of 0.25 m is selected. Due to the complexity of the vessel and the configuration of the refractory inside the reactor, a factor of 4 for installation (fins) is considered. The refractory used in the calculations has a density of 2700 kg/m3 and a cost estimated at 700 €/ton (2022).

$$c_{refractory} = 0.7 \cdot t \cdot A \cdot \rho_{ref} \cdot f_{inst} \quad (30)$$

Insulation costs were estimated as 12 % of the purchased equipment cost, based on typical values reported in Plant Design and Economics for Chemical Engineers for equipment and piping insulation in chemical plants, and assumed applicable to the present system. The cost of reactor internals was calculated following the component-based approach of [26], [27]. The value chosen is 25% of the reactor cost and serves as a conservative mid-range estimate, given an internal cost range of 15% to 40% of the reactor cost. The internal cost varies with the mechanical complexity of the reactor architecture (fixed or fluidised bed) and the high-temperature requirements. Fluidised systems tend to be more expensive due to complex distributors and cyclones.

For the cost of electric heaters, values in the literature correspond to conventional system operating below 800 ºC. A reference cost of 175 – 300 €/kW is present in the literature [31], [32]. At higher temperatures (~1200 ºC), substantial cost increases are expected due to the transition to advanced heating elements (e.g., SiC or $MoSi_2$). studies on electric furnace design and standard cost estimation methodologies [26], [27] indicate that changes in materials and design typically increase costs by a factor of 2–4.

The reference cost of industrial electric heaters (175–300 €/kW) corresponds to conventional systems operating below 800 ºC. At higher temperatures (~1200 ºC), substantial cost increases are expected due to the transition to advanced heating elements (e.g., SiC or $MoSi_2$) and the need for high-grade refractory insulation. Although direct cost correlations with temperature are not explicitly available in the literature, studies on electric furnace design and standard cost estimation methodologies [26], [27] indicate that such changes in materials and design typically lead to cost increases. Accordingly, a correction factor of 2 and a cost of 300 €/kW were adopted.

$$c_{electric} = 600 \cdot P_{elec}^{0.7} \quad (31)$$

The reactor configuration includes an internal heat exchanger for energy transfer. The cost of the heat exchange unit integrated into the reactor system was estimated using the modular factoring method established by[27]. Considering the extreme operating environment (maximum temperature of around 1200 ºC), the base purchase cost, derived from empirical correlations (year: 1990) for shell-and-tube configurations, was adjusted through a multi-factor integration. A material factor (F_m = 5) was assigned to reflect the requirement for high-nickel superalloys, such as Inconel. A design factor (f_d = 1.25) to accommodate a floating-head architecture necessitated by differential thermal expansion was used. The pressure factor (fp = 1.1) accounts for the additional cost of a 15 bar design. An overall heat transfer coefficient of around 50–300 W/(m^2· K) is expected [33]. Base calculation was done for a thermal power transfer of 1MW$_t$ and a heat transfer coefficient of 50 W/(m2· K).

$$c_{heat\ exchanger} = 190 \cdot Q(kW)^{0.6} \cdot f_{mat} \cdot f_d \cdot f_p \qquad (33)$$

$$c_{heat\ exchanger} = 190 \cdot Q(kW)^{0.6} \cdot 5 \cdot 1.25 \cdot 1.1 = 1308 \cdot Q(kW)^{0.6} \qquad (34)$$

Overall equation:

$$c_{reactor} = 1.37 \cdot [4220 \cdot A^{0.6} + 1890 \cdot A + 600 \cdot P_{elec}(kW_e)^{0.7} + 1308 \cdot Q(kW_t)^{0.6}] \qquad (35)$$

Since the presented cost estimation model deviates from conventional thermal power scaling and relies on physically grounded assumptions, a sensitivity analysis was conducted to assess the impact of parameter uncertainties. The variables selected for evaluation are those operating under the highest technical and economic uncertainty due to the extreme temperature conditions of the calcium looping process. Specifically, the material factor for the high-nickel superalloy heat exchanger (f_{mat}), the cost multiplier for advanced electric heating elements, and the internal refractory installation complexity f_{inst} were varied. Additionally, standard commodity fluctuations for the steel shell and refractory material were included to account for market volatility.

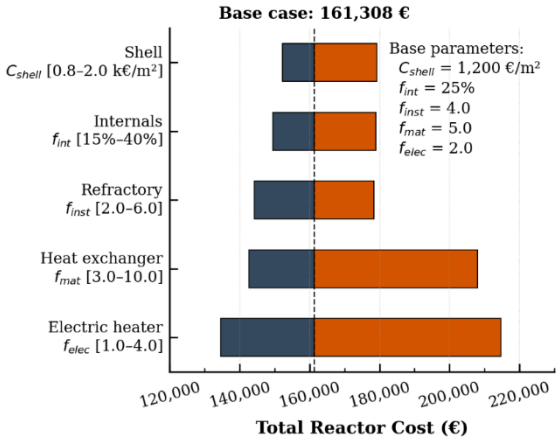

Figure 6 *Sensitivity analysis for reactor cost*

The thermoeconomic response of the reactor cost architecture highlights a clear decoupling between process-specific thermal parameters and auxiliary structural variables. Commodity-dependent indicators, namely the shell unit cost (C_{shell}) and the internals allowance (f_{int}), have a minor impact on the total investment, indicating that uncertainty in generic structural manufacturing is a secondary risk. Conversely, the economic feasibility of the system is intensely constrained by the core high-temperature components. Conservative variations in the heat exchanger material factor (f_{mat}) and the electric heater multiplier (f_{elec}) expand the total CAPEX up to approximately 208,100 € and 214,600 €, respectively. This behaviour validates the proposed physically grounded cost-decomposition methodology, demonstrating that for advanced fixed-bed thermochemical architectures operating under high-temperature conditions (~1200 °C), the financial risk is fundamentally dominated by metallurgical-grade scaling and specialised heating technologies rather than by conventional volumetric or energy-capacity scaling correlations.

3.2. Auxiliar equipment cost

Beyond the main reactor, the capital expenditures for the auxiliary equipment—including heat exchangers, gas storage units, and solids handling mechanisms—are detailed in Table 2. To ensure a representative economic evaluation aligned with recent economic conditions, all baseline costs have been updated using the Chemical Engineering Plant Cost Index (CEPCI [34]). This indexing ensures a consistent and standardized baseline for inflation adjustment. The cost (C_{year}) of each equipment is calculated following the equation 32.

$$C_{year} = C_{year\ ref} \cdot \frac{CEPCI_{year}}{CEPCI_{year\ ref}} \qquad (36)$$

Where CEPCI year ref represents the index value corresponding to the original cost reference year, and $CEPCI_{year}$ the index for the target evaluation year. For this study, the economic baseline has been set to 2024, utilizing the June 2024 CEPCI value of 798.8.

Table 2 *Equipment cost*

Equipment	Correlation	Year	CEPCI	Ref
Turbine	$4001 \cdot Turbine\ Power^{0.6897}$	2017	567,5	[35]
Compressor	$643.15 \cdot Compressor\ Power^{0.9142}$	2017	567,5	[35]
Storage tank	$C_{ss}\left(\frac{€}{kg}\right) \cdot \rho_{ss}\left(\frac{kg}{m^3}\right) \cdot V_{ss}(m^3)$	2018	603,1	[36]
Heat exchanger A	$32.3 \cdot Heat\ exchanged\ (kW)$	2005	468,2	[37]
Heat exchanger B	$3197 \cdot HX\ Area^{0.67} \cdot Pressure^{0.28}$	2005	468,2	[37]
Limestone	$m_{CaCO_3} \cdot C_{CaCO_3}\left(\frac{€}{kg}\right)$	-	-	[24]

3.3. Levelised cost of heat

To evaluate the long-term economic competitiveness of the proposed modular single-reactor system, the Levelised Cost of Heat (LCOH) is utilized as the primary financial metric. This indicator aggregates all capital and operational expenditures incurred over the lifetime of the plant, normalized by the total thermal energy delivered to the industrial process. The LCOH (€/MWhth) is formulated in equation:

$$LCOS\left(\frac{€}{MWh}\right) = \frac{TCR \cdot FCF + OPEX}{ATE} + LCOE_{PV/Wind} \quad (37)$$

$$FCF = \frac{r \cdot (1+r)^t}{(1+r)^t - 1} \quad (38)$$

Where TCR represents the Total Capital Requirement (detailed in Annex 1). The Fixed Charge Factor (FCF – Equation 34) is used to annualise the initial capital investment. The OPEX accounts for the annual operational and maintenance expenditures, while ATE is the Annual Thermal Energy (MWhth) effectively delivered by the thermochemical storage system to the industrial application. LCOE accounts for the levelised cost of the renewable electricity consumed during the charging stage, adapted to the specific hybrid PV–wind configurations of each evaluated European region. The economic lifespan of the project (t) is assumed to be 25 years, a standard duration for industrial-scale thermal infrastructure. A discount rate (r) of 6% is adopted as a realistic baseline for energy transition projects in Europe under current macroeconomic conditions. This financial framework allows for a consistent comparison of the thermal energy costs across the selected locations, capturing the trade-offs between regional renewable potential and system utilization factors.

4. Case study

To ensure the scalability and generalizability of the proposed thermochemical energy storage (TCES) systems, six European locations—Seville (Spain), Lyon (France), Frankfurt (Germany), Rome (Italy), Warsaw (Poland), and Stockholm (Sweden)—were strategically selected to represent a comprehensive latitudinal transect. This selection captures the full spectrum of Europe's climatic archetypes, ranging from the high-irradiance, PV-dominant Mediterranean basin to the wind-abundant, high-latitude Northern regions. By encompassing diverse solar-to-wind ratios and contrasting seasonal thermal demand profiles, these sites provide a robust framework to evaluate the techno-economic performance of TCES in decarbonizing medium-to-high temperature industrial processes under heterogeneous renewable resource availability.

The photovoltaic plant was modelled with System Advisory Model (SAM) software [38]. Meteorological data is

extracted from the “Photovoltaic Geographical Information System” (PVGIS project) [39], considering a Typical Meteorological Year (TMY). The power plant is 10 MWdc, utilizing a 1-axis tracking system to optimize solar resource capture throughout the day. The installation incorporates crystalline silicon modules with a nominal cell efficiency of 21% (0.21) and a temperature coefficient of -0.35%/°C. To maximize inverter utilization. The raw power output is converted into net power output by accounting for standard miscellaneous system losses (14%) and a progressive annual module degradation rate of 0.5% over the plant operating period, determining the final net electricity available for the process.

For the economic assumptions of the solar PV system, an initial capital expenditure (CAPEX) of 850 €/kW is considered, together with fixed operation and maintenance (O&M) costs of 15 €/kW·year. The system lifetime is assumed to be 25 years, and a discount rate of 6% is applied. Based on these parameters, the capital recovery factor (CRF) is calculated as 0.0782.

The hourly wind power generation profile was retrieved from the Renewables.ninja platform REF. This tool converts MERRA-2 REF reanalysis weather data into power output by considering specific technical parameters such as turbine hub height and power curves, and has been extensively validated against measured data across Europe. For this study, the wind farm configuration was modeled with a total capacity of 10 MW, utilizing Vestas V150-4000 turbines at a hub height of 120 m. The raw gross power output was converted into net power output by accounting for standard operational and technical penalties, which include aerodynamic wake losses (10%), electrical transmission losses (2%), and plant availability constraints (3%). These parameters result in a cumulative loss factor of 0.856, which was applied to determine the final net electricity available for the process.

For the economic assumptions of the wind power system, an initial capital expenditure (CAPEX) of 1400 €/kW is considered, together with fixed operation and maintenance (O&M) costs of 40 €/kW·year. The system lifetime is assumed to be 25 years, and a discount rate of 6% is applied. Based on these parameters, the capital recovery factor (CRF) is calculated as 0.0782, which is used to annualise the investment cost and ensure a consistent integration within the overall economic assessment of the energy storage system.

The study proposes heat supply via the production of 1 kg/s of superheated steam (15 bar) at a temperature of 400 °C. The thermal power is 2.41 MWt. Assuming a heat transfer efficiency of 90% for the designed system, the total required thermal supply is 2.68 MWt. Two heat demand scenarios have been considered: one where demand occurs daily from 06:00 to 22:00, and another with a continuous 24-hour demand. For the energy supply, a 10 MW photovoltaic plant and a 10 MW wind power plant have been considered. The following energy supply scenarios have been studied, ensuring the total plant capacity remains fixed at 10 MW:

- 100 % photovoltaic.
- 75 % photovoltaic and 25 % wind.
- 50 % photovoltaic and 50 % wind.
- 25 % photovoltaic and 75 % wind.
- 100 % wind.

The techno-economic assessment (TEA) of the thermochemical energy storage (TCES) system is initiated by evaluating the localised cost of the driving renewable electricity supply. For this analysis, identical capital expenditures (CAPEX) and operational expenditures (OPEX) are assumed across all regions to maintain a consistent baseline, with both photovoltaic (PV) and wind installations sized at a nominal capacity of 10 MW each. PV systems are modelled at 850 €/kW CAPEX and 15 €/kW·year OPEX, whilst wind assets are evaluated at 1,400 €/kW CAPEX and 40 €/kW·year OPEX. Operating under a 25-year economic lifetime and a 6% discount rate, the resulting Levelised Cost of Electricity (LCOE) depends directly on the specific annual production profile of each location.

Table 3 *Energy supply. Production and cost*

	Sevilla	Lyon	Frankfurt	Roma	Varsovia	Estocolmo
PV production (GWh)	18,1	14,1	10,7	15,9	10,6	10,4
LCOE PV (€/MWh)	45,0	57,7	76,0	51,1	76,9	78,3
Wind production (GWh)	30,7	26,3	23,6	23,8	29,2	35,9
LCOE Wind (€/MWh)	48,6	56,8	63,3	62,8	51,1	41,7

As detailed in Table 3, geographical variations significantly govern renewable generation performance. Southern latitudes, led by Seville, achieve the highest PV yields (18.1 GWh) and the lowest PV LCOE (45.0 €/MWh), whereas lower solar irradiation in northern locations (Stockholm and Warsaw) raises costs to 78.3 €/MWh. Conversely, this trend is reversed for wind generation: northern maritime and continental regimes offer higher yields, with Stockholm recording the lowest wind LCOE (41.7 €/MWh), while lower wind resources in Frankfurt and Rome increase levelised costs to 63.3 €/MWh and 62.8 €/MWh, respectively. For hybridised configurations, the comprehensive LCOE is calculated in proportion to the nominal capacity share allocated to

each technology. Consequently, the combined levelised cost scales linearly with the single-source baselines, depending on the specific power-mix ratios.

This section presents results on the temporal alignment between renewable energy production and industrial demand at both daily and monthly levels, along with the associated levelised cost of heat. Using this matching framework, the following analysis evaluates the operational viability, storage-charging dynamics, and economic feasibility of the proposed system across the selected industrial benchmarks.

4.1. Results and discussion

This section presents the techno-economic results of the proposed modular calcium looping system, focusing on the Levelised Cost of Heat (LCOH) calculated for six European locations. The economic performance is evaluated and compared under two distinct operating schedules: a continuous 24-hour industrial heat demand and a staggered 16-hour profile running from 06:00 to 22:00. These cases highlight how the temporal distribution of the thermal load interacts with regional photovoltaic and wind availability to determine the final cost of the delivered heat.

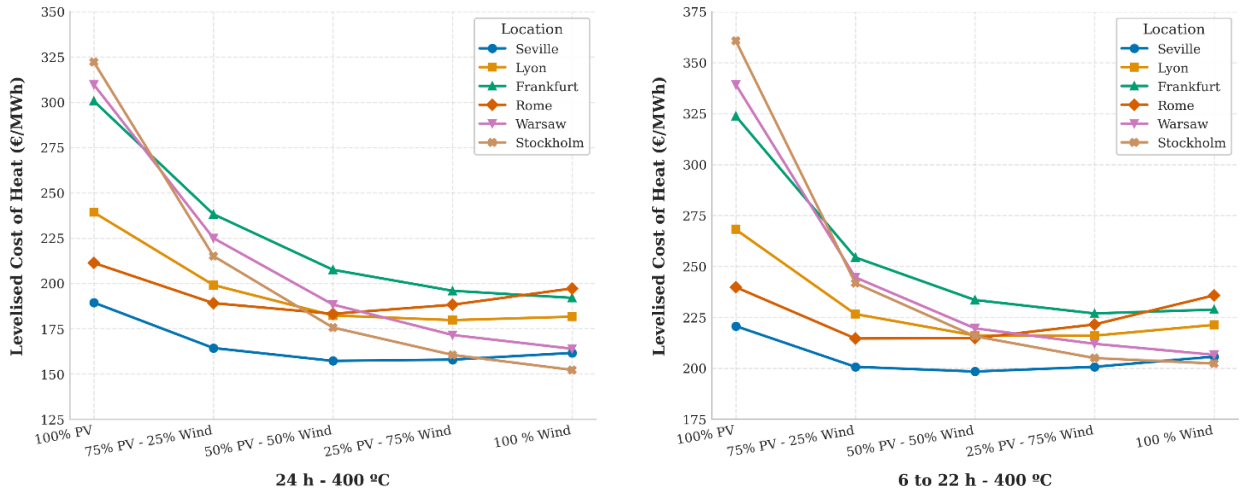

Figure 7 *Levelised cost of heat for (a) 24 h and (b) 6 to 22 h heat demand*

Figure 7a presents the levelised cost of heat (LCOH) across the six evaluated European locations under a continuous 24-hour industrial demand profile. A clear downward trend in energy costs is observed for central and northern European hubs—such as Frankfurt, Warsaw, and Stockholm—as the renewable mix transitions from 100% photovoltaic (PV) toward wind-dominated configurations, with Stockholm achieving its minimum cost of approximately 152 €/MWh under a 100% wind scenario. This behaviour is directly linked to the higher winter wind yields and the superior production capacity of wind assets, which continue generating electricity during nocturnal hours to complement the steady, round-the-clock baseload thermal demand far more effectively than solar inputs. Conversely, Mediterranean locations like Seville and Rome exhibit a distinct economic profile; Seville achieves its lowest thermal cost of 157.2 €/MWh at a balanced 50% PV and 50% wind configuration, beyond which increasing the wind share yields diminishing economic returns due to the exceptional and highly reliable solar resource available in Southern Europe. Overall, these results demonstrate that mitigating the LCOH for continuous industrial operations relies heavily on optimising the regional renewable generation mix to prevent excessive over-sizing of the storage inventory by exploiting nighttime resource availability.

Figure 7b illustrates the levelised cost of heat (LCOH) for the staggered 16-hour industrial demand profile operating from 06:00 to 22:00, revealing a noticeable increase in energy costs across all locations when compared to the continuous 24-hour baseline. This economic penalty is directly attributable to the lower annual thermal energy effectively delivered by the system in this configuration, which reduces the plant's capacity factor and limits the amortisation of significant upfront capital expenditures (CAPEX). For instance, in solar-dependent configurations (100% PV), the LCOH for northern hubs like Stockholm and Warsaw spikes significantly above 325 €/MWh, whereas the 24-hour continuous operation allowed these same locations to maintain a lower cost floor. Although integrating wind capacity successfully mitigates these peaks due to its higher production capacity and nocturnal availability, the overall LCOH curves remain systematically shifted upwards compared to the round-the-clock scenario, demonstrating that maximising system utilisation is critical to reducing the levelised cost of thermochemical heat delivery.

To unravel the underlying financial mechanisms of the proposed system, the total LCOH is decoupled into its two primary components: the levelised cost of the driving renewable electricity and the levelised cost associated with the modular calcium looping reactor inventory. Figure 8 illustrates this cost breakdown across the six European locations for the continuous 24-hour and the staggered 16-hour operational profiles,

respectively. While the absolute capital and operational expenditures of the modular reactor remain constant across all scenarios, its levelised contribution (€/MWh) varies directly with the total annual thermal energy effectively delivered to the industrial process, thereby shifting the economic weight of each component depending on regional resource integration.

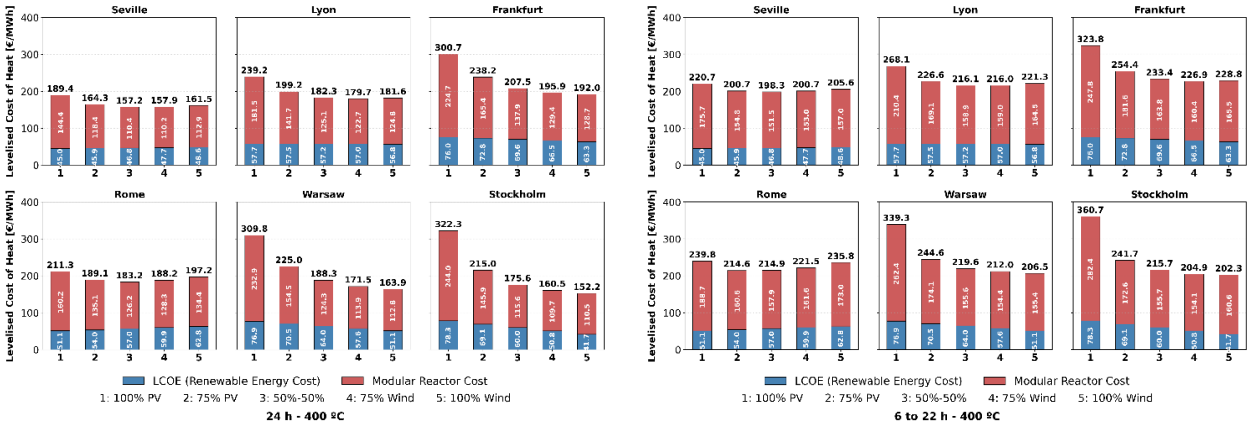

Figure 8 *Cost contribution for each scenario in (a) 24 h and (b) 6 to 22 h heat demand*

The cost breakdown reveals that the levelised reactor cost acts as an indicator of system utilisation and capacity factor. In solar-dependent configurations (Case 1) in high-latitude regions such as Stockholm and Warsaw, the limited annual thermal output causes fixed reactor costs to spike dramatically, exceeding €200/MWh and dominating the LCOH structure. Conversely, as the energy mix transitions toward wind-dominated shares (Cases 4 and 5), the higher capacity factors and extended operating hours effectively dilute these fixed capital charges, minimising the reactor's levelised contribution to its floor limit. This dilution effect is severely compromised under the staggered 16-hour profile (Figure 8b), where the enforced compression of the discharging window prevents full asset amortisation, consequently inducing a systematic upward shift in the levelised reactor cost across all geographical archetypes regardless of the driving electricity source.

Figure 9 displays the monthly demand fulfilment rate across the six European locations under the continuous 24-hour operational profile, with a required thermal load of 1.92 GWh per month. A clear trend emerges, highlighting the seasonal vulnerability of purely solar-driven systems (Case 1: 100% PV), which suffer severe generation deficits during the winter months, even in Southern European climates, and drop below 15% in central and northern hubs such as Frankfurt, Warsaw, and Stockholm. Conversely, transitioning the generation matrix toward wind-dominated configurations (Case 5: 100% Wind) improves reliability across regions, allowing Seville, Warsaw, and Stockholm to maintain high coverage rates close to 100% throughout the winter. This high performance is directly tied to the superior production capacity and nocturnal availability of wind assets in these regions. However, this trend is not uniform across the continent, as locations such as Frankfurt and Rome still experience noticeable supply shortfalls during the spring and summer months, underscoring that regional climate characteristics dictate the ultimate effectiveness of storage charging cycles.

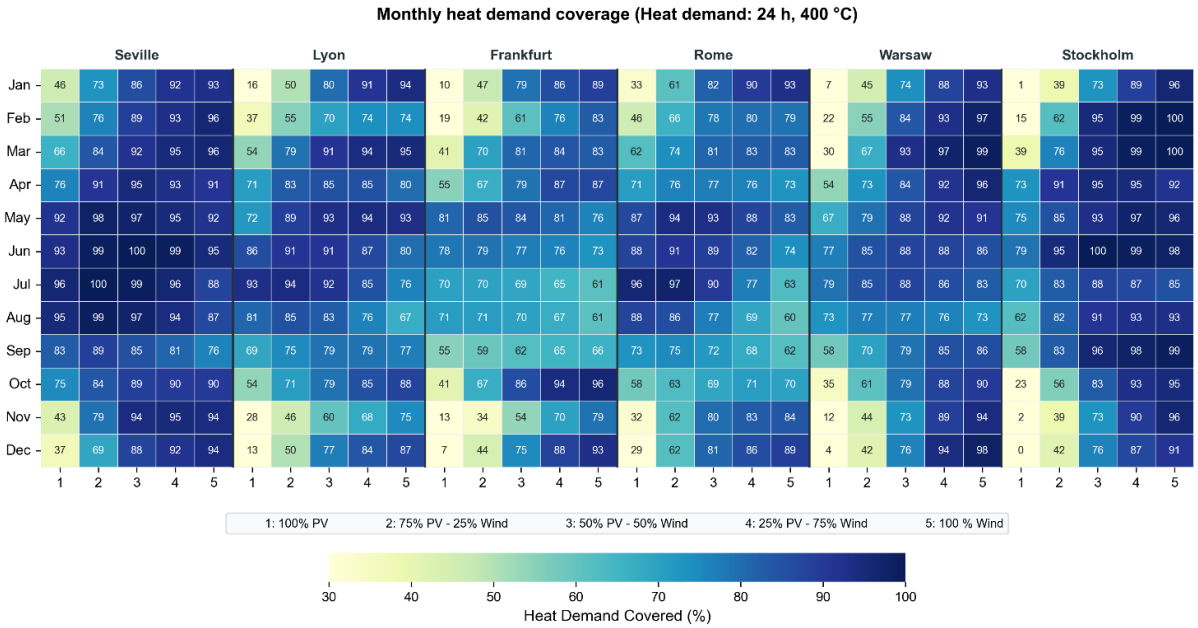

Figure 9 *Monthly heat demand coverage for 24 h heat demand*

A detailed analysis of the monthly demand fulfilment rate under the staggered 16-hour profile (Figure 10) reveals a distinct shift in generation dynamics when compared to the 24-hour baseline, particularly for solar-reliant systems (Case 1: 100% PV). In this case, the monthly heat demand is 1.3 GWh. In Mediterranean regions like Seville and Rome, concentrating the industrial load within daytime hours substantially compresses the supply gap, allowing pure solar configurations to achieve or come remarkably close to 100% coverage during spring and summer by avoiding the extensive nocturnal storage discharges required by round-the-clock operations. However, this daytime alignment is insufficient to mitigate the harsh winter deficits in Central and Northern European locations, where Case 1 still falls below 25% due to severe seasonal resource limitations. On the other hand, under wind-dominated configurations (Case 5: 100% Wind), Stockholm, Warsaw, and Seville maintain a highly stable coverage profile that stays close to 100%. Conversely, Rome and Frankfurt exhibit worse behaviour under wind configurations, experiencing noticeable supply contractions during the summer period, underscoring how compressing the demand window can restrict the integration window for non-coincident renewable yields, depending on local weather patterns.

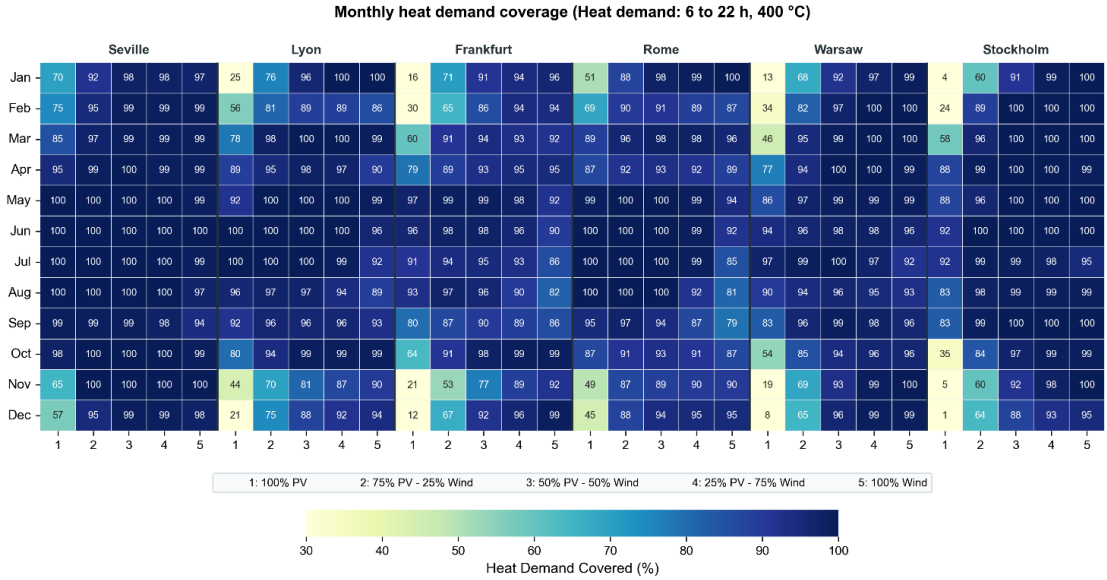

Figure 10 *Monthly heat demand coverage for 6 to 22 h heat demand*

Operational efficiency is strictly constrained by the volume of renewable generation that is curtailed once the system reaches its physical storage capacity. This thermal curtailment occurs when the calcium looping bed reaches its maximum temperature threshold of 1100 °C, which forces the termination of the charging phase and results in unexploited excess energy. Figure 11 quantifies this energy across each evaluated scenario.

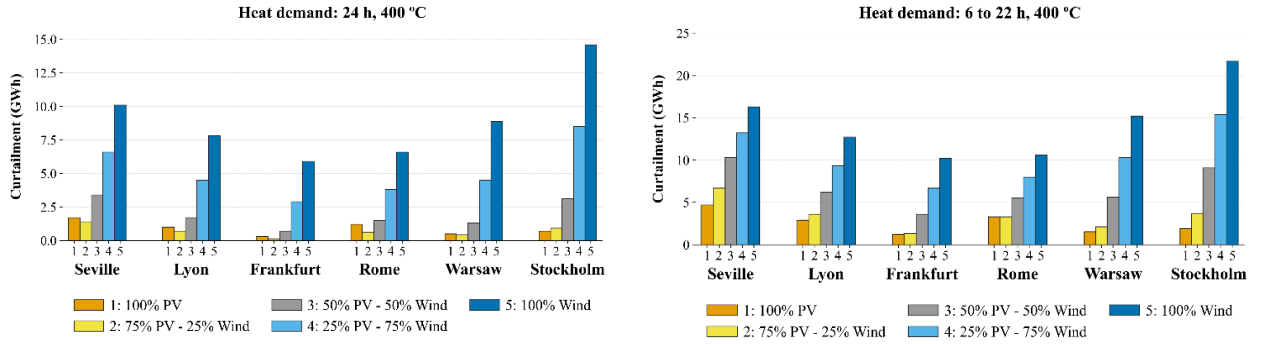

Figure 11 *Curtailment for (a) 24 h and (b) 6 to 22 h heat demand*

As illustrated in Figure 11, electrical curtailment scales significantly as the generation matrix transitions from solar-dominated to wind-dominated configurations (Cases 1 to 5) across all evaluated locations. This trend is driven by the higher annual capacity factors and sustained peak generation profiles of the 10 MW wind assets, which frequently generate large electricity surges that saturate the reactor's maximum thermal capacity. Furthermore, a comparative assessment reveals a systematic increase in energy curtailment when shifting from a continuous 24-hour thermal demand to a staggered 16-hour operational window.

5. Conclusions

This study established a spatially resolved framework for a modular single-reactor Calcium Looping configuration, demonstrating its high-potential capability to supply high-grade industrial steam optimised for real, high-demand, high-temperature processes. The economic maps reveal that the Levelized Cost of Heat (LCOH) is not uniform but spans a competitive, highly viable range of 150-175 €/MWh across most analysed regions, fluctuating dynamically as a function of the local renewable energy scenario. Mitigating these costs fundamentally depends on continuous 24-hour operations to maximise asset amortisation, with wind-dominated northern configurations and solar-abundant southern corridors, such as Seville, presenting balanced and outstanding feasibility pathways.

To evaluate these configurations beyond rigid empirical estimates, a physically grounded cost-decomposition methodology was developed to establish a robust parametric cost-calculation capability. This flexible parametric approach uncovers a structural decoupling between process energy metrics and economic sensitivities, demonstrating that capital investment risks are highly concentrated in critical high-temperature components and electric heating elements rather than in conventional volumetric scaling laws. Baseline calculations, validated at an initial renewable capacity of 10 MW, demonstrate that the LCOH values are highly competitive for this technology stage and highlight significant potential for further cost reductions as the project scale and primary renewable capacity expand.

While this assessment provides a solid baseline for industrial defossilization, real manufacturing gates expose vital avenues for system optimisation. First, static thermal baseloads must be replaced with dynamic, batch-dependent fluctuations in industrial heat demand. Second, replacing flat renewable energy costs with dynamic intra-day electricity pricing will allow calcination cycles to target pricing valleys, reducing operational expenditures. Crucially, future architectures must transition toward a decentralised energy management framework enabling simultaneous, staggered charging and discharging sequences across a distributed network of modular reactors. This advanced scheduling will prevent all units from operating concurrently, optimising overall exergy efficiency and guaranteeing a flexible, uninterrupted thermal supply.

Acknowledgment

This work has been partially developed within the project Procesos y componentes para el almacenamiento híbrido de energía térmica basado en sales fundidas y carbonatos (PID2022- 140815OB-C21) funded by the Spanish Ministry of Science and Innovation; the project ‘Renewable Methanol-based Synthetic Multifuel Production (METHCESFUEL)’, funded by the European Commission through Horizon, the EU Framework Programme for Research and Innovation, under Grant Agreement No. 101235215; and the project Desarrollo de reactor/intercambiador de alta eficiencia para sistema de almacenamiento de energía termoquímico basado en la reacción de hidratación del óxido de calcio (DGP_PIDI_2024_01538) funded by the Regional Government of Andalusia (Consejería de Universidad, Investigación e Innovación) and co-funded by the European Union.

Annex

Table 4 *TCR's breakdown [40], [41]*

Parameter	Estimation
Piping	3% Equipment Purchase
Electrical costs	3% Equipment Purchase
Instrumentation	4% Equipment Purchase
Total Purchase Equipment	Equipment Purchase + Piping + Electrical + Instrumentation
Material costs	3% Total Purchase Equipment
Labour	5% Total Purchase Equipment
Bare Erected Cost	Total Purchase Cost + Material + Labour
Engineering Cost	3% Bare Erected Cost
EPC Cost	Bare Erected Cost+Engineering Cost
Project Contingencies	10% EPC Cost
Process Contingencies	10% EPC Cost
TPC	EPC Cost+Project Cont+Process Cont
Owner's Cost	2% TPC
TCR	TPC + Owner's Cost

References

[1] "Heat – Renewables 2023 – Analysis - IEA." Accessed: Jun. 17, 2026. [Online]. Available: https://www.iea.org/reports/renewables-2023/heat

[2] K. M. Adamson *et al.*, "High-temperature and transcritical heat pump cycles and advancements: A review," *Renewable and Sustainable Energy Reviews*, vol. 167, p. 112798, Oct. 2022, doi: 10.1016/J.RSER.2022.112798.

[3] C. Arpagaus, F. Bless, M. Uhlmann, J. Schiffmann, and S. S. Bertsch, "High temperature heat pumps: Market overview, state of the art, research status, refrigerants, and application potentials," *Energy*, vol. 152, pp. 985–1010, Jun. 2018, doi: 10.1016/J.ENERGY.2018.03.166.

[4] S. Collins, P. Deane, B. Ó Gallachóir, S. Pfenninger, and I. Staffell, "Impacts of Inter-annual Wind and Solar Variations on the European Power System," *Joule*, vol. 2, no. 10, pp. 2076–2090, Oct. 2018, doi: 10.1016/j.joule.2018.06.020.

[5] N. Ahmed, K. E. Elfeky, L. Lu, and Q. W. Wang, "Thermal and economic evaluation of thermocline combined sensible-latent heat thermal energy storage system for medium temperature applications," *Energy Convers. Manag.*, vol. 189, pp. 14–23, Jun. 2019, doi: 10.1016/J.ENCONMAN.2019.03.040.

[6] C. Prieto, P. Cooper, A. I. Fernández, and L. F. Cabeza, "Review of technology: Thermochemical energy storage for concentrated solar power plants," *Renewable and Sustainable Energy Reviews*, vol. 60, pp. 909–929, Jul. 2016, doi: 10.1016/J.RSER.2015.12.364.

[7] R. Chacartegui, A. Alovisio, C. Ortiz, J. M. Valverde, V. Verda, and J. A. Becerra, "Thermochemical energy storage of concentrated solar power by integration of the calcium looping process and a CO2 power cycle," *Appl. Energy*, vol. 173, pp. 589–605, Jul. 2016, doi: 10.1016/j.apenergy.2016.04.053.

[8] S. M. Hashemi, M. H. Sedghkerdar, and N. Mahinpey, "Calcium looping carbon capture: Progress and prospects," *Canadian Journal of Chemical Engineering*, vol. 100, no. 9, pp. 2140–2171, Sep. 2022, doi: 10.1002/cjce.24480.

[9] C. Ortiz, R. Chacartegui, J. M. Valverde, J. A. Becerra, and L. A. Perez-Maqueda, "A new model of the carbonator reactor in the calcium looping technology for post-combustion CO2 capture," *Fuel*, vol. 160, pp. 328–338, Nov. 2015, doi: 10.1016/J.FUEL.2015.07.095.

[10] R. Chacartegui *et al.*, “Carbonation tests in a kW-scale entrained flow reactor for thermochemical energy storage using the calcium looping-based system,” *Chemical Engineering Journal*, vol. 524, Nov. 2025, doi: 10.1016/j.cej.2025.169801.

[11] J. Blamey, E. J. Anthony, J. Wang, and P. S. Fennell, “The calcium looping cycle for large-scale CO2 capture,” Apr. 2010. doi: 10.1016/j.pecs.2009.10.001.

[12] M. Angerer *et al.*, “Design of a MW-scale thermo-chemical energy storage reactor,” *Energy Reports*, vol. 4, pp. 507–519, Nov. 2018, doi: 10.1016/J.EGYR.2018.07.005.

[13] C. Ortiz, J. M. Valverde, R. Chacartegui, L. A. Pérez-Maqueda, and P. Gimenez-Gavarrell, “Scaling-up the calcium-looping process for co2 capture and energy storage,” *KONA Powder and Particle Journal*, vol. 38, pp. 189–208, 2021, doi: 10.14356/kona.2021005.

[14] V. Gjorgievski, S. Cundeva, N. Markovska, and N. Duić, “IndustryHeat-EU: Harmonized Dataset of Industrial Final and Useful Energy Demand by Temperature Level for EU27 and Member States”, doi: 10.5281/ZENODO.17414346.

[15] W. L. Luyben, “Design and Control of the Styrene Process,” *Ind. Eng. Chem. Res.*, vol. 50, no. 3, pp. 1231–1246, Feb. 2010, doi: 10.1021/IE100023S.

[16] A. Tarafder, G. P. Rangaiah, and A. K. Ray, “Multiobjective optimization of an industrial styrene monomer manufacturing process,” *Chem. Eng. Sci.*, vol. 60, no. 2, pp. 347–363, Jan. 2005, doi: 10.1016/J.CES.2004.07.120.

[17] A. K. Y. Yee, A. K. Ray, and G. P. Rangaiah, “Multiobjective optimization of an industrial styrene reactor,” *Comput. Chem. Eng.*, vol. 27, no. 1, pp. 111–130, Jan. 2003, doi: 10.1016/S0098-1354(02)00163-1.

[18] S. Mesfun and A. Toffolo, “Optimization of process integration in a Kraft pulp and paper mill – Evaporation train and CHP system,” *Appl. Energy*, vol. 107, pp. 98–110, Jul. 2013, doi: 10.1016/J.APENERGY.2013.02.016.

[19] E. Cortés and W. Rivera, “Exergetic and exergoeconomic optimization of a cogeneration pulp and paper mill plant including the use of a heat transformer,” *Energy*, vol. 35, no. 3, pp. 1289–1299, Mar. 2010, doi: 10.1016/J.ENERGY.2009.11.011.

[20] E. Mateos-Espejel, L. Savulescu, F. Maréchal, and J. Paris, “Base case process development for energy efficiency improvement, application to a Kraft pulping mill. Part II: Benchmarking analysis,” *Chemical Engineering Research and Design*, vol. 89, no. 6, pp. 729–741, Jun. 2011, doi: 10.1016/J.CHERD.2010.09.013.

[21] P. Pardo, A. Deydier, Z. Anxionnaz-Minvielle, S. Rougé, M. Cabassud, and P. Cognet, “A review on high temperature thermochemical heat energy storage,” *Renewable and Sustainable Energy Reviews*, vol. 32, pp. 591–610, Apr. 2014, doi: 10.1016/J.RSER.2013.12.014.

[22] G. Alva, Y. Lin, and G. Fang, “An overview of thermal energy storage systems,” Feb. 01, 2018, *Elsevier Ltd*. doi: 10.1016/j.energy.2017.12.037.

[23] R. Salgado-Pizarro, A. Calderón, A. Svobodova-Sedlackova, A. I. Fernández, and C. Barreneche, “A multi-scale experimental study on calcium-looping for thermochemical energy storage using the CO2 captured from power generation systems,” *J. Energy Storage*, vol. 86, p. 111400, May 2024, doi: 10.1016/j.est.2022.104377.

[24] C. Ortiz, J. M. Valverde, R. Chacartegui, L. A. Perez-Maqueda, and P. Giménez, “The Calcium-Looping (CaCO3/CaO) process for thermochemical energy storage in Concentrating Solar Power plants,” Oct. 01, 2019, *Elsevier Ltd*. doi: 10.1016/j.rser.2019.109252.

[25] F. J. Durán-Olivencia, J. M. P. Ebri, M. J. Espín, and J. M. Valverde, “The cohesive behavior of granular solids at high temperature in solar energy storage,” *Energy Convers. Manag.*, vol. 240, Jul. 2021, doi: 10.1016/j.enconman.2021.114217.

[26] G. P. . Towler and R. K. . Sinnott, *Chemical engineering design : principles, practice and economics of plant and process design*. Butterworth-Heinemann is an imprint of Elsevier, 2022.

[27] K. A. Kobe, “Plant design and economics for chemical engineers (Peters, Max S.),” *J. Chem. Educ.*, vol. 35, no. 10, p. A506, Oct. 1958, doi: 10.1021/ED035PA506.

[28] E. W. McAllister, “Pipeline Rules of Thumb Handbook: A Manual of Quick, Accurate Solutions to Everyday Pipeline Engineering Problems,” *Pipeline Rules of Thumb Handbook: A Manual of Quick, Accurate Solutions to Everyday Pipeline Engineering Problems*, pp. 1–791, Sep. 2013, doi: 10.1016/C2013-0-00277-0.

[29] P. Sengupta, “Refractories for the Chemical Industries,” *Refractories for the Chemical Industries*, pp. 1–377, Nov. 2020, doi: 10.1007/978-3-030-61240-5/SAVE-RESEARCH.

[30] C. A. SCHACHT, “REFRACTORY LININGS,” Pittsburgh, Pennsylvania, 1995.

[31] J. Rissman, “Decarbonizing Low-Temperature Industrial Heat in the U.S.,” Oct. 2022. Accessed: Jun. 02, 2026. [Online]. Available: https://energyinnovation.org/wp-content/uploads/Decarbonizing-Low-Temperature-Industrial-Heat-In-The-U.S.-Report-2.pdf

[32] “Forest Sector Net-Zero Roadmap Phase II: Catalogue of key decarbonization actions.” Accessed: Jun. 02, 2026. [Online]. Available: https://www.wbcsd.org/wp-content/uploads/2024/04/WBCSD_Catalogue-of-key-decarbonization-actions.pdf

[33] M. Angerer *et al.*, “Design of a MW-scale thermo-chemical energy storage reactor,” *Energy Reports*, vol. 4, pp. 507–519, Nov. 2018, doi: 10.1016/j.egyr.2018.07.005.

[34] “The Chemical Engineering Plant Cost Index ® - Chemical Engineering.” Accessed: Mar. 26, 2026. [Online]. Available: https://www.chemengonline.com/pci-home

[35] M. D. Carlson, B. M. Middleton, and C. K. Ho, “PowerEnergy2017-3590 TECHNO-ECONOMIC COMPARISON OF SOLAR-DRIVEN SCO2 BRAYTON CYCLES USING COMPONENT COST MODELS BASELINED WITH VENDOR DATA AND ESTIMATES.”

[36] A. Bayon *et al.*, “Techno-economic assessment of solid–gas thermochemical energy storage systems for solar thermal power applications,” *Energy*, vol. 149, pp. 473–484, Apr. 2018, doi: 10.1016/j.energy.2017.11.084.

[37] S. Michalski, D. P. Hanak, and V. Manovic, “Techno-economic feasibility assessment of calcium looping combustion using commercial technology appraisal tools,” *J. Clean. Prod.*, vol. 219, pp. 540–551, May 2019, doi: 10.1016/j.jclepro.2019.02.049.

[38] National Renewable Energy Laboratory, “System Advisor Model Version 2017.1.17 (SAM 2017.1.17),” 2024, *Golden, CO*.

[39] European Commission, “Photovoltaic Geographical Information System (PVGIS).”

[40] E. De Lena *et al.*, “Techno-economic analysis of calcium looping processes for low CO2 emission cement plants,” *International Journal of Greenhouse Gas Control*, vol. 82, pp. 244–260, Mar. 2019, doi: 10.1016/j.ijggc.2019.01.005.

[41] R. Turton, R. C. Bailie, W. B. Whiting, J. A. Shaeiwitz, and D. Bhattacharyya, “Analysis, Synthesis, and Design of Chemical Processes Fourth Edition”.